# 3-D SEISMIC RESPONSE OF LIQUEFACTION-SUSCEPTIBLE IMPROVED-SOIL DEPOSITS

**Brendon BRADLEY**, Institute of Science and Engineering, Chuo University
1-13-27, Kasuga, Bunkyo-ku, Tokyo 112-8551, JAPAN
Email: *brendon.bradley@canterbury.ac.nz*
**Kazuhiro ARAKI**, Design Department, Chemical Grouting Co. Ltd.
2-2-5, Toranomon, Minato-ku, Tokyo 105-0001, JAPAN
*Email: k-araki@chemicalgrout.co.jp*
**Takeshi ISHII**, Institute of Science and Engineering, Chuo University
1-13-27, Kasuga, Bunkyo-ku, Tokyo 112-8551, JAPAN
Email: *t-ishii@kc.chuo-u.ac.jp*
**Kunio SAITOH**, Department of Civil and Environmental Engineering, Chuo University
1-13-27, Kasuga, Bunkyo-ku, Tokyo 112-8551, JAPAN
*Email: saitoh@civil.chuo-u.ac.jp*

***Keywords*:** seismic response, liquefaction, jet grouting ground improvement, stress-density model

**SUMMARY**

Numerous earthquakes occurring over the last five decades have illustrated the significant hazards posed by soil liquefaction. Recent observations have also illustrated the potential hazard mitigation that can be achieved by reducing soil liquefaction potential via ground improvement technologies. Despite these observations, there remain many challenges in ground improvement, both in innovative improvement technologies themselves, and also in prediction of the seismic performance of improved soil deposits. This paper presents the results of an investigation into the seismic response of liquefiable soil deposits which utilize various configurations of soil improvement using seismic effective stress analysis. The particular problem considered is based on the soil stratigraphy of the downhole seismic array at Port Island, Kobe, and the input ground motion used is that which was recorded at this location in the great 1995 Kobe earthquake. Firstly we compare the observed ground motion during the 1995 Kobe earthquake with those obtained based on 1 dimensional (1-D) analysis. Secondly, we present the salient results of 3-D finite element analyses using various soil improvement configurations. Finally, comparison is made of the results of the set of analyses as a function of improvement area ratio in an effort to identify which types of improvement configuration is most effective at mitigating the consequences of soil liquefaction.

## 1. PROBLEM CONSIDERED

Soil liquefaction, which results from a build-up of excess pore water pressures in loose saturated soils, leads to an almost complete loss of strength and stiffness of soil and consequently unacceptably large deformations. Figure 1 illustrates the extensive region over which liquefaction occurred at Port Island during the 1995 Kobe earthquake.

The effects of soil liquefaction on strong ground motion can be understood by examining the strong ground motions recorded at various depths at the Port Island seismic array (see Figure 1) which are shown in Figure 2. The soil profile at the seismic array is shown in Figure 3. It can be seen that the incoming ground motion at a depth of 32m has a peak acceleration of 0.6g, and that the intensity and frequency content of the ground motion is preserved in propagating through alluvial gravel and clay soils

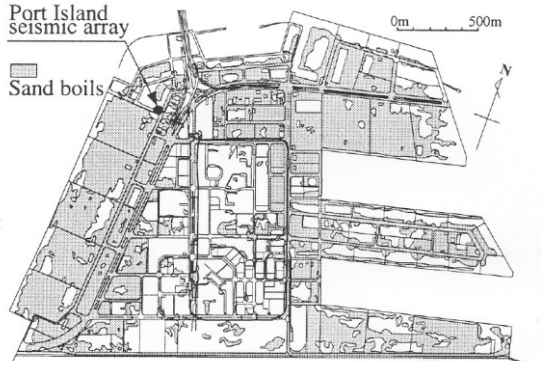


**Figure 1 Liquefaction observed in the 1995 Kobe earthquake and the location of the seismic array at Port Island.**

from 32m depth to 16m depth. On the other hand, the ground motion observed at the surface (GL-0m) is notably different from those observed at depth, with a significant reduction in acceleration amplitude and removal of high frequency ground motion at t=5s.

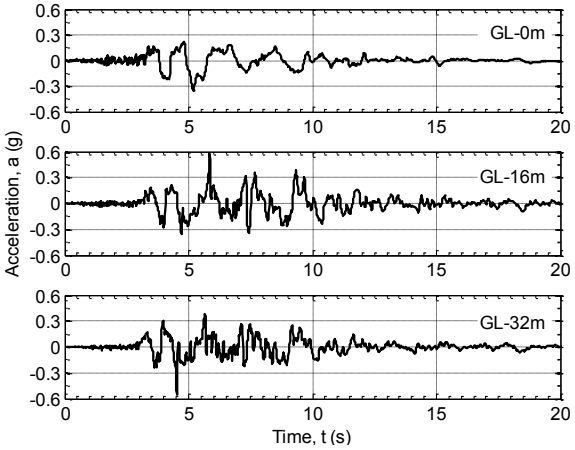


**Figure 2 Observed ground motion at the Port Island array in the 1995 Kobe earthquake**

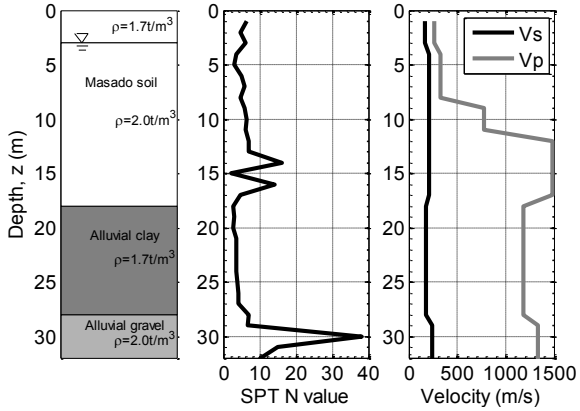


**Figure 3 Soil properties at Port Island seismic array**

In order to illustrate the physical mechanisms which result in the observations in Figure 2, as well as the capability to model them, a finite element analysis of a single column of soil was performed. The alluvial gravel and clay were modeled as elastic materials, while the sand layer of Masado soil was modeled using the elastic-plastic Stress-Density (S-D) model of Cubrinovski and Ishihara [1998]. The S-D model parameters adopted for Masado soil are given in Table 1.

**Table 1 Stress-density model parameters used for Masado soil [Cubrinovski et al., 2000]**

| | | | |
|---|---|---|---|
| Elastic | $A$=199 | $n$=0.80 | $\nu$=0.10 |
| Stress-strain | $(\tau/p')_{max}$ | $G_{N,max}$ | $G_{N,min}$ |
| | $a_1$=0.745 | $a_2$=332 | $a_3$=180 |
| | $b_1$=0.10 | $b_2$=60 | $b_3$=10 |
| State index | UR-line | Steady state line | |
| | $e_0$=0.430 | $e_s$=0.464-0.051$lnp'$ | |
| Stress-dilatency | $\mu_0$=0.18 | $M$=0.75 | $S_c$=0.012 |

Figure 4 compares the predicted acceleration time histories at the ground surface and 15m depth with those observed. It can be seen that the model is able to capture the key features of the seismic response of the soil deposits.

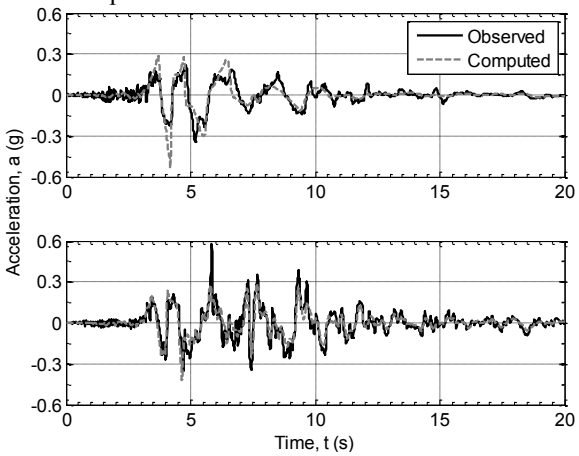


**Figure 4 Comparison of observed and predicted ground motion at the Port Island array**

Figure 5 illustrates the seismic response of the Masado soil at a depth of 10.5m. Figure 5 illustrates that excess pore pressures rapidly develop after the onset of strong ground motion shaking at approximately 3s, and liquefaction first occurs at approximately 5s (for which the excess pore water pressure ratio, EPWPR, is equal to 1.0). Figure 5 also illustrates the stress path, and stress-strain response of the soil. It can be seen that as the effective stress of the soil decreases the shear stiffness and strength of the soil also rapidly decrease.

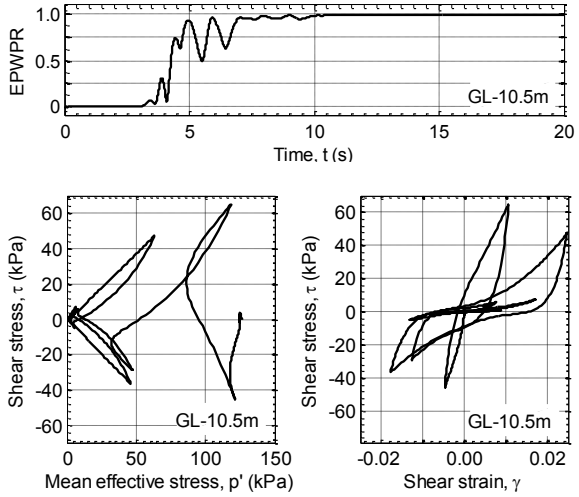


**Figure 5 Illustration of pore pressure development, stress path, and stress-strain response of soil at depth of GL-10.5m**

## 2. FINITE ELEMENT MODEL WITH GROUND IMPROVEMENT

The seismic performance of soil deposits can be improved using various ground improvement

techniques. Jet grouting is one such technique which involves the horizontal injection of cementitious material into the soil under high pressures. Rotation of the injection nozzle allows for the formation of a circular section (in plan) of improved soil, and by overlapping such sections, walls or cells of improved soil can be formed. The increased stiffness and strength of improved soil using the jet grouting method can enhance the seismic performance of nearby native soils by providing kinematic constraints on the deformation of such soils, and therefore mitigate the effects of excessive liquefaction of such deposits when subjected to strong ground motion.

A key consideration in the use of jet grouting (and other improvement techniques) is the determination of an appropriate geometry of improved cells or walls. Obviously such a consideration involves a balance between the improved seismic performance, and increased cost associated with a larger volume of grout injection. However, because the improved soil provides kinematic constraint to the surrounding native soil, it is possible that different improved soil geometries with the same total improved area may provide different levels of performance improvement. In an effort to investigate such a question, nine different geometries of soil improvement were considered for a hypothetical site of overall plan dimensions of 24m by 24m. Table 2 provides a list of the different improvement geometries considered, while Figure 6 provides schematic illustrations of the geometries in plan-view. In summary, three different cell configurations were considered: 1 cell, 4 cell, and 9 cell. For each cell configuration, different wall widths were selected. For each of the 8 cases considered, the improved area ratio, $R_{IA}$, defined as the ratio of improved to total soil area (in plan). It is noted that $R_{IA}$ for the different wall widths for each cell configuration are essentially equal, implying approximately equal material costs in construction. Because the potentially liquefiable soil layer extends from the ground surface to 18m depth, the top 18m of soil was considered for ground improvement.

**Table 2 Details of improved soil geometries**

| Case ID | No. of cells | Wall width, $W$ (m) | Improved area ratio, $R_{IA}$ |
|---|---|---|---|
| 1C-2 | 1 | 2.0 | 0.31 |
| 1C-3 | 1 | 3.0 | 0.44 |
| 1C-4 | 1 | 4.0 | 0.56 |
| 4C-1.5 | 4 | 1.5 | 0.34 |
| 4C-2 | 4 | 2.0 | 0.44 |
| 4C-2.5 | 4 | 2.5 | 0.53 |
| 9C-1 | 9 | 1.0 | 0.31 |
| 9C-1.5 | 9 | 1.5 | 0.44 |
| 9C-2 | 9 | 2.0 | 0.56 |

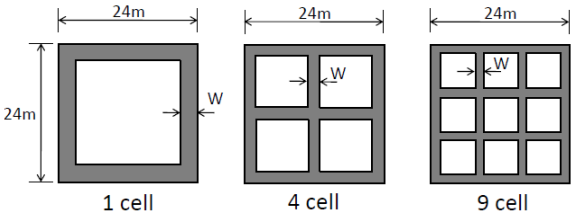


**Figure 6 Considered improved soil geometries**

Figure 7 illustrates the finite element mesh which was used for performing the various analysis cases considered. Firstly, it should be noted that use was made of symmetry about the X-axis to reduce computational demands. The same vertical stratigraphy as that for the Port Island seismic array was considered. The 3-D effective stress modeling of the Masado soil layer was based on a simplified approach in which pore-pressures were assumed to occur only due to deformation in the principal plane of response (i.e. the x-z plane), and that the response is governed by three-independent shear mechanisms [Cubrinovski et al., 2003]. The improved soil was modeled as a linear elastic material with shear stiffness of $E$=420MPa.

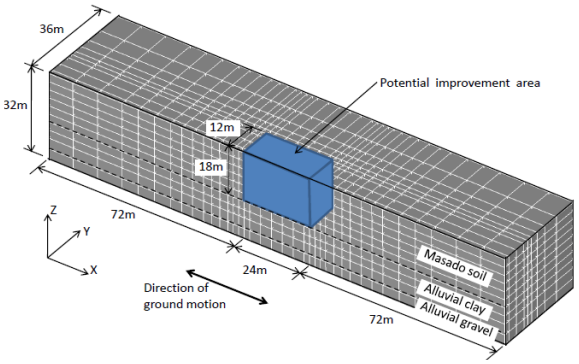


**Figure 7 Schematic illustration of the finite element model used indicating the area considered for ground motion improvement (note that X-symmetry was employed)**

## 3. RESULTS OF 3-D EFFECTIVE STRESS ANALYSES

As previously noted, a total of 9 different soil improvement geometries were considered. Below, we consider two cases for each number of cells considered in order to demonstrate the salient effects of how the improved soil region affects the dynamic response of the soil deposit. Finally, we summarize the results by comparing all cases based on the improved area ratio.

### 3.1. Response of soil inside improved region

In order to illustrate the effects of ground improvement on seismic response consider firstly the response of the soil deposit enclosed within the improved area. Figure 8 compares the acceleration and displacement histories of ground surface at the

centre of the soil enclosed within the improved soil region. It can be seen that for the first cycle of strong ground motion, the response is similar for the unimproved and two improved cases, however subsequent to this the aforementioned degradation in stiffness and strength of the soil in the unimproved case leads to reduced acceleration amplitudes, longer vibration period, and larger peak displacements. On the other hand, the ground improved cases do not show such characteristics. The response for the considered soil improvement cases is similar, but it is noted that the peak displacement, which occurs at approximately t=5s, is slightly lower for the 1C-4 case as compared to the 1C-2 case.

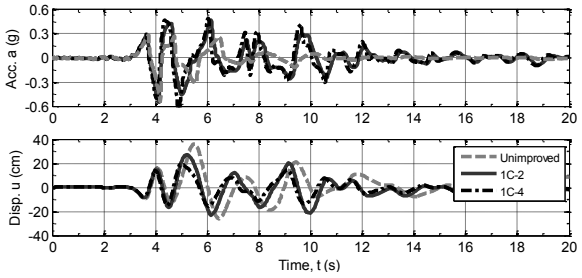


**Figure 8 Acceleration and displacement at the ground surface for two wall widths in the 1 cell case**

Figure 9 illustrates the acceleration response spectra of the ground motion presented in Figure 8. As previously noted it can be seen that in the unimproved case the spectral amplitudes are notably less than the ground improvement cases for $T<3$ seconds. Interestingly, the reduction in the peak ground acceleration is small, as this occurs early in the response time history, while the peak acceleration response for 1 second period, which requires several cycles of strong ground motion to achieve resonance, is significantly larger in the improved cases.

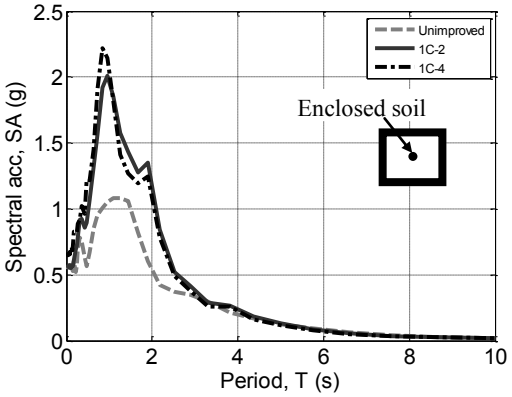


**Figure 9 Acceleration response spectra of the surface ground motion for two wall widths in the 1 cell case. (5% critical damping)**

Figure 10 illustrates the response of soil at a depth of 10.5m for the two different soil improvement geometries in comparison to the unimproved case. It can be seen that for the 1C-2 case, liquefaction occurs at essentially the same time as in the unimproved case, however the consequent cyclic shear strains induced are significantly less. In comparison, in the 1C-4 case the occurrence of liquefaction is delayed by several seconds as pore pressures build up at a slower rate. It can be seen that, while complete liquefaction eventually develops in the 1C-4 case, the induced cyclic strains are notably smaller than in the 1C-2 and unimproved cases.

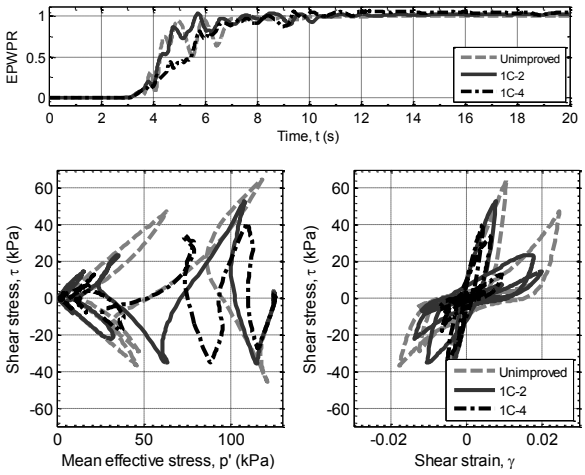


**Figure 10 Pore pressure development, stress path, and stress-strain response of soil at depth of GL-10.5m for two wall widths in the 1 cell case**

Figure 11 illustrates the distribution with depth of peak accelerations, displacements and shear strains at the centre of the soil enclosed in the improved cell. Firstly, it can be seen that shear strains are largest in the Masado soil layer (i.e. depths<18m), with peak shear strains below 0.5% in the underlying alluvial gravel and clay layers. It can also be seen that peak shear strains of nearly 3% occur in the unimproved case compared with 2% in the 1C-2 soil improvement case and 1% in the 1C-4 case. At the ground surface the previously discussed shear strains translate to peak displacements of 36cm, 27cm, and 19cm, for the unimproved, 1C-2, and 1C-4 cases, respectively. It is also pertinent to note that, in terms of peak accelerations, the soil improvement cases generally lead to an increase in peak accelerations in the Masado soil layer, and a reduction in the alluvial gravel and clay layers as a result of less "trapping" of waves in the surface layer.

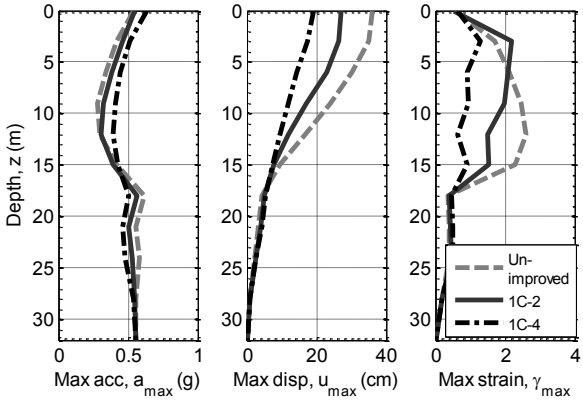


**Figure 11 Maximum acceleration, displacement, and shear strain with depth at the centre of the 1 cell improved region**

### 3.2. Response of improved soil cell

Figure 12 illustrates the displacement with depth of the centre and edge of the improved soil cell, as well as its displacement in plan along the perpendicular face. It can be firstly seen that in the 1C-2 case (i.e. cell width of 2m and length 24m) the differential displacement of the cell wall in plan is significant with the centre of the cell undergoing almost the same displacement as the free-field soil, while the displacement at the cell edges is on the order of half that of the free-field. In the 1C-4 case (i.e. twice the wall width of the 1C-2 case) it can be seen that the differential displacement in plan is less pronounced with peak displacements of approximately 18cm and 16cm at the centre and edge of the cell, respectively. It can also be seen that in the 1C-4 case, and at the cell edge in the 1C-2 case, the displacement with depth is approximately linear, implying approximately constant strain with depth in the improved soil. Finally it is noted that due to the stiffness of the improved soil, the peak displacements at the base of the improved soil edge are greater than that of the surrounding soil, as previously observed by others in the case of deep-soil-mixing (DSM) ground improvement walls [Cubrinovski et al., 2003].

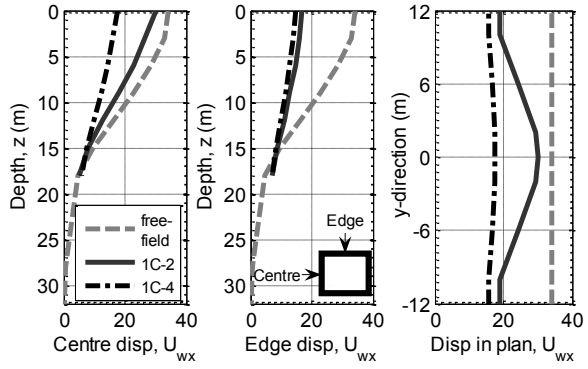


**Figure 12 Displacements of improved soil centre and edge with depth and displacement in plan (1 cell case)**

### 3.3. Features of the response in the 4 cell case

There are several similarities between the responses of the improved ground in the 4 cell cases and those of the 1 cell cases, and hence discussion here is only given to the notable differences between these.

The surface acceleration and displacement response at the centre of the improved zone in the 4 cell cases was essentially identical to that observed in the 1 cell case (i.e. Figure 8). Figure 13 illustrates the soil response within the improved soil cell at a depth of 10.5m. Unlike the 1C-2 case shown in Figure 10, it can be seen that even for the thin cell wall (i.e. 1.5m) the response in the 4C-1.5 case illustrates that the generation of excess pore pressures occurs at a reduced rate compared with that in the unimproved case. In the 4C-2.5 case, in particular, it can be seen that complete liquefaction (i.e. *EPWPR*=1.0) does not occur at a depth of 10.5m, and hence significantly lower peak shear strains occur.

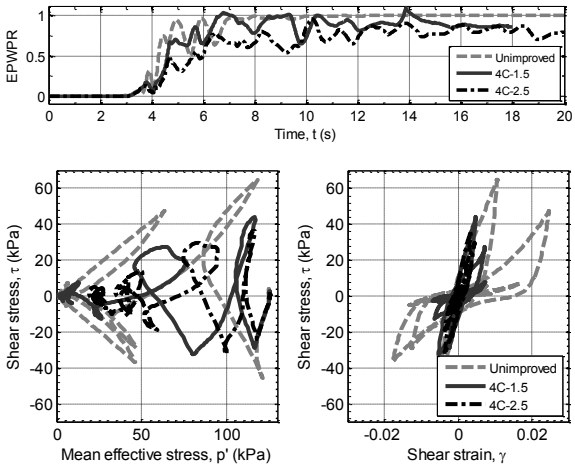


**Figure 13 Pore pressure development, stress path, and stress-strain response of soil at depth of GL-10.5m for two wall widths in the 4 cell case**

Figure 11 illustrates the peak acceleration, displacement and shear strains with depth at the centre of the 4 cell improved region. Similar, to the results observed in the 1 cell case, it can be seen that soil improvement leads to an increase in peak accelerations in the Masado soil layer, and reduced accelerations in the underlying alluvial gravel and clay layers. It can be seen that displacement and shear strains in the improved cases are similar, and significantly less than the unimproved case. In particular peak surface displacements in both the 4C-1.5 and 4C-2.5 cases are less than 20cm compared with 36cm in the unimproved case. In the 4C-2.5 case, for which as previously noted complete liquefaction does not occur, it can be seen that the peak shear strains are approximately 0.5% which is similar to those in the underlying gravel and clay layers. For the 4C-1.5 case it can be seen that the occurrence of increased pore pressures, particularly at the base of the Masado soil layer, leads to larger shear strains.

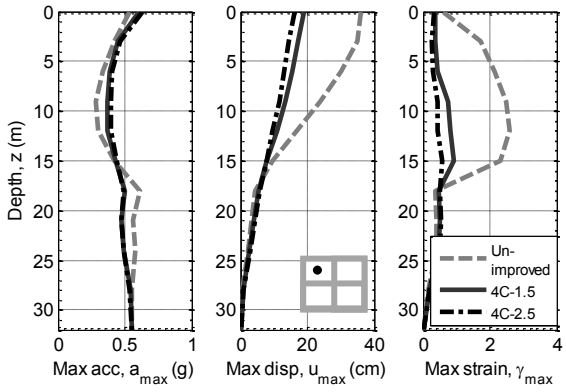


**Figure 14 Maximum acceleration, displacement and shear strain with depth at the centre of the 4 cell improved region**

Figure 15 illustrates the peak displacement with depth at the middle of the perpendicular improved soil cell wall as well as the peak displacements in plan at the ground surface. It can be seen that in the 4C-1.5 case there is some difference in peak displacements in plan, although not as significant as was observed in the 1C-2 case (Figure 12). In contrast, the variation in the displacements in plan for the 4C-2.5 case is very small. The displacements with depth at the centre of the wall are similar to those observed in the 1 cell case.

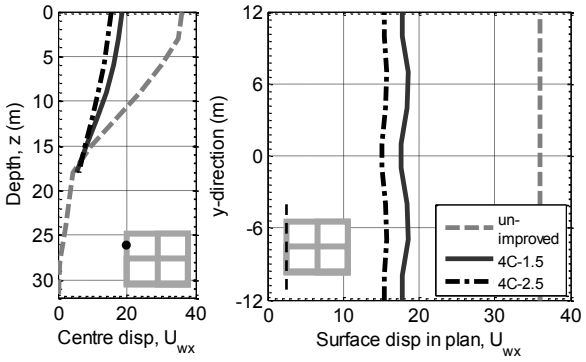


**Figure 15 Displacements of improved soil centre-line with depth and displacement in plan (4 cell case)**

### 3.4. Features of the response in the 9 cell case

Figure 16 illustrates the time history of excess pore water pressure ratio within the improved cell at a depth of 10.5m. While liquefaction occurs at approximately t=5s in the unimproved case, it can be seen that liquefaction is delayed until approximately t=6.5s in the 9C-1 case, and liquefaction does not fully occur in the 9C-2 case (at this depth).

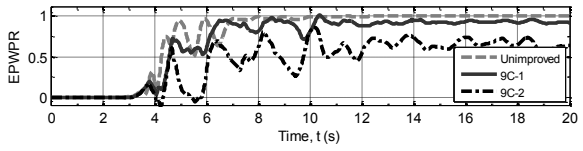


**Figure 16 Pore pressure development at a depth of GL-10.5m for two wall widths in 9 cell case**

Figure 17 illustrates the peak acceleration, displacement and shear strains with depth at the centre of the 9 cell improved region. It can be seen that the results in the 9 cell case are very similar to the results presented for the two 4 cell geometries in Figure 14.

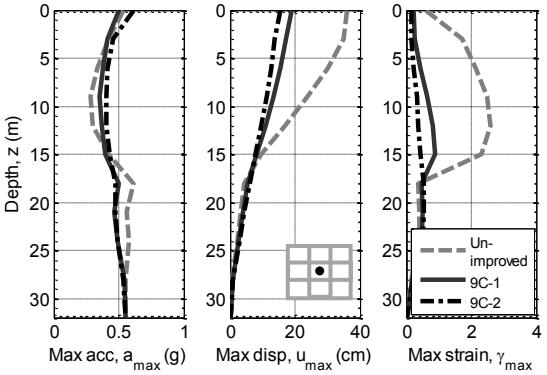


**Figure 17 Maximum acceleration, displacement and shear strain with depth at the centre of the 4 cell improved region**

Figure 18 illustrates the peak displacement with depth at the middle of the perpendicular improved soil cell wall as well as the peak displacements in plan at the ground surface. Similar to the observations for the 4 cell cases presented in Figure 15, it can be seen that in the 9C-1 case there is a small difference in peak displacements in plan, while the variation for the 9C-2 case is negligible.

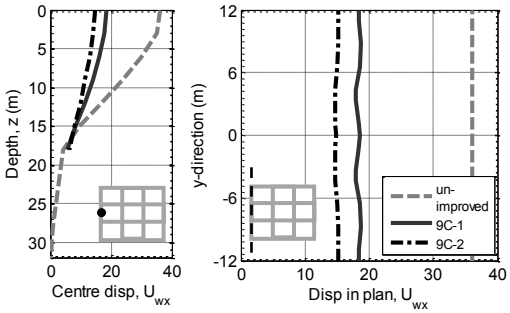


**Figure 18 Displacements of improved soil centre-line with depth and displacement in plan (4 cell case)**

### 3.5. Summary of effect of soil improvement geometries in terms of improved area ratio, $R_{IA}$

In order to summarize the effect of soil improvement, and in particular the relative merits of the 9 different improvement geometries considered, in this section various parameters of response are examined as a function of improved soil ratio. As previously noted, the improved soil ratios for the different improved geometries are given in Table 1.

Figure 19 illustrates the peak ground displacement of surface soil enclosed within the improved region as a function of the improved area ratio. Firstly, it can be seen that all 9 improvement geometries are

effective with displacements in the range 15-27cm, as compared to the 36cm displacement in the unimproved case. For a given number of cells it can be seen that there is a reduction in peak displacement with increasing improvement ratio. Finally, it can be seen that for a given improvement ratio the 9 cell configuration results in the lowest displacements, followed by the 4 cell case.

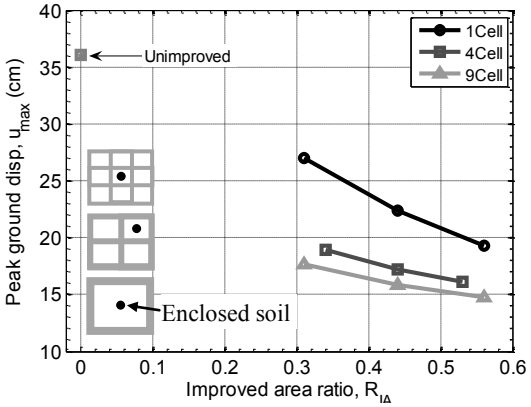


**Figure 19 Variation in peak surface ground displacement of soil inside the improved area**

Figure 20 illustrates the peak displacements at the centre of the perpendicular walls of the improved region as a function of improved area ratio. As noted above, it can be seen that for a given improved area ratio the lowest wall displacements are observed for the 9 cell case, although the displacements in the 4 cell case are also similar. As was observed in Figure 12, there is a significant difference between the different wall widths considered in the 1 cell case.

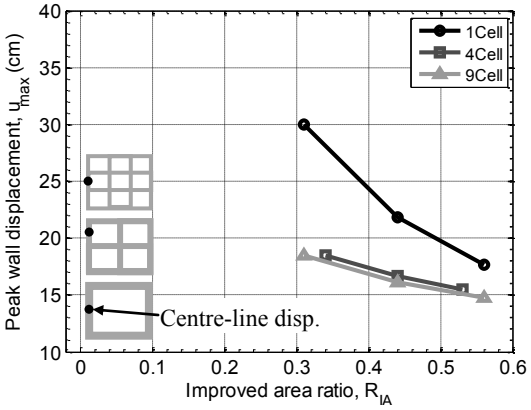


**Figure 20 Variation in peak surface ground displacement along the centre-line of the improved cell**

Figure 21 illustrates the peak displacements at the edge of the parallel walls of the improved region as a function of improved area ratio. It can be seen that improved area ratio is a good metric for this measure of response with all three cases essentially falling onto a unique line.

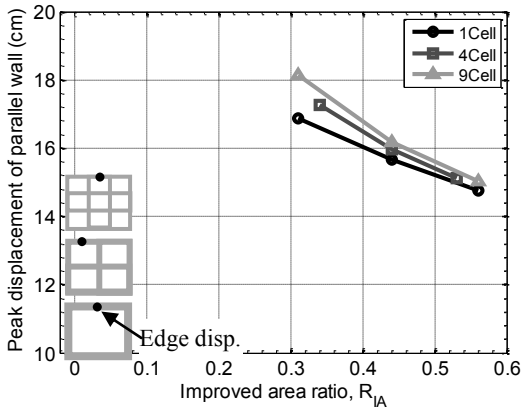


**Figure 21 Variation in peak surface ground displacement along the edge of the improved cell**

It was previously noted, in relation to Figure 9, that the use of soil improvement results in an increase in spectral accelerations for short to moderate vibration periods. This increase in spectral accelerations is important as it mean that increased seismic demands will result for structures which are founded on improved soils. Figure 22 illustrates the variation in spectral accelerations as a function of improved area ratio. As previously noted, it can be seen that there is little difference between the peak ground acceleration in the improved and unimproved cases, but that the SA(0.5) and SA(1.0) amplitudes are much larger with ground improvement. In the 1 cell case it can be seen that increasing the improved area (i.e. increasing the wall width) leads to an increase in spectral amplitudes, while the effect of increasing wall thickness on spectral amplitudes is relatively small for the 4 and 9 cell cases.

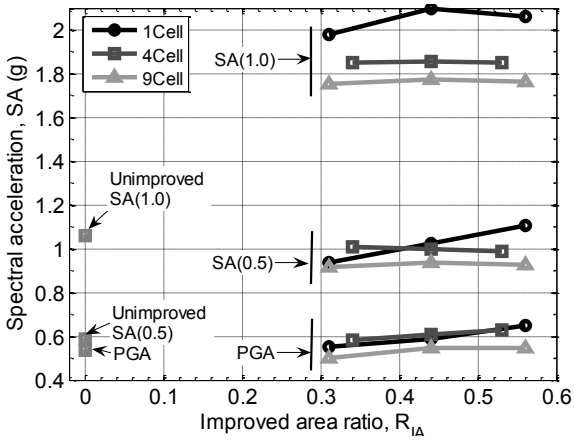


**Figure 22 Variation in peak spectral acceleration at the surface inside the improved area**

Interestingly, it can be seen that for all three vibration periods (0.0, 0.5, and 1.0s) the lowest spectral amplitudes in Figure 22 result when using the 9 cell ground improvement configuration, and the largest when using the 1 cell ground improvement. It is inferred that this observation is the result of waveguide effects. In the 1 cell case the incoming

seismic waves are "guided" to the surface within the improved region. On the other hand, the smaller dimensions of unimproved soil enclosed within each cell in the 9 cell case means that this waveguide phenomena is less pronounced with the entire enclosed soil tending to move with the improved soil as a unit.

One possible reason for the different peak displacements of the enclosed soil and at the centre-line of the improved wall for the different cell configuration could be a result of the fact that, for a given improved area, the ratio of cell length to cell width is different for the different cell configurations. Figure 23 illustrates the ratio of the cell clear length to cell width, L/W, as a function of improved area ratio for the different cell geometries considered. It can be seen that for a given improved area ratio the 9 cell configuration leads to smaller L/W ratio, followed by the 4 cell and 1 cell configurations. It can be seen that the correlation observed in Figure 23 is similar to that in Figure 19 and Figure 20 giving further credence to the possibility that L/W affects the seismic response characteristics.

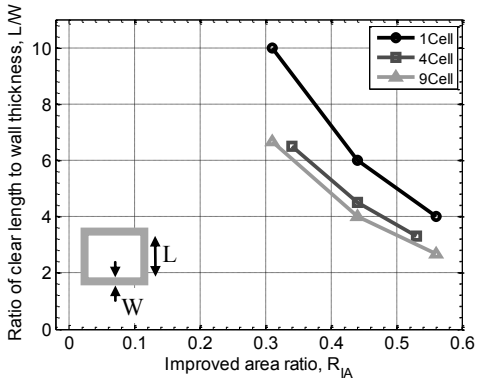


**Figure 23 Relationship between improved area ratio and wall length to width ratio, L/W**

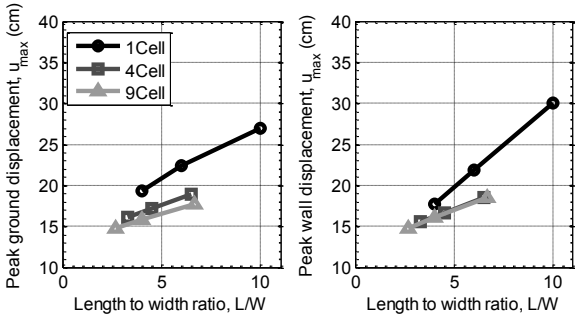


**Figure 24 Peak ground and wall displacements as a function of length to width ratio, L/W**

Figure 24 presents the same results for enclosed soil and wall centre-line displacements as presented in Figure 19 and Figure 20, but as a function of L/W. It can be seen that there is a relatively good correlation between L/W and centre-line wall displacement with the 9 and 4 cell configurations essentially coincident. On the other hand, there is still a discrepancy between the peak displacements of the enclosed soil as a function of L/W for the different cell configurations. This suggests the ratio L/W alone cannot fully describe the salient feature of the observed responses.

## 4. DISCUSSION

The aforementioned analyses have illustrated the benefits of soil improvement on the seismic performance of soil deposits susceptible to liquefaction within a limited scope. Further research is required to more carefully understand the implications of the non-linear stress-strain modeling of the improved soil, as well as the effects of soil improvement on overlying superstructures and their foundations.

Finally, the consideration of 3-D non-linear finite element analyses requires extremely large computational resources. The present analyses were limited to relatively coarse finite element meshes in order to limit the number of nodes, and hence computational demands. Hence, there is clear need for such finite element analysis programs to be implemented in parallel formulation for super-computer application so that computational problems with finer scale finite element meshes can be computed in realistic time frames.

## 5. CONCLUSIONS

This paper has presented the results of 3-D seismic effective stress analyses to investigate the effect of various ground improvement configurations on seismic response of liquefiable soils. The results clearly indicate the effectiveness of the ground improvement and also the utility of advanced analyses to ascertain the key features of the seismic response.

## 6. ACKNOWLEDGMENTS

Funding of the first author from the Japan Society for the Promotion of Science (JSPS) is greatly appreciated. Discussions on various matters with Prof. K. Ishihara are greatly appreciated.

## 7. REFERENCES

Cubrinovski, M., Ishihara, K., (1998). "State concept and modified elastoplasticity for sand modelling", *Soils and foundations*, Vol.38, No.4, pp.213-225.

Cubrinovski, M., Ishihara, K., Furukawazono, K., (2000). "Analysis of two case histories on liquefaction of reclaimed deposits", *Proc. of 12th World Conference on Earthquake Engineering* Auckland, New Zealand.

Cubrinovski, M., Ishihara, K., Shibayama, T., (2003). "Seismic 3-D effective stress analysis: constitutive modelling and application", *Proc. of Deformation Characteristics of Geomaterials*, D. B. e. al., Editor: Lyon, France. pp.8.